Published in final edited form as:
Sci Signal. ; 6(273): ra28.1–15. doi:10.1126/scisignal.2003884.

Epigenetic Activation of AP-1 Promotes Squamous Cell Carcinoma Metastasis

Xiangming Ding[1,*], **Hongya Pan**[1,5,*], **Jiong Li**[1], **Qi Zhong**[1,6], **Xiaohong Chen**[1,6], **Sarah M. Dry**[3,7], and **Cun-Yu Wang**[1,2,3,4,†]

[1]Laboratory of Molecular Signaling, Division of Oral Biology and Medicine, School of Dentistry, University of California at Los Angeles, Los Angeles, California 90095, USA

[2]Department of Bioengineering, Henry Samueli School of Engineering and Applied Science, University of California at Los Angeles, Los Angeles, California 90095, USA

[3]Jonsson Comprehensive Cancer Center, University of California at Los Angeles, Los Angeles, California 90095, USA

[4]Eli and Edythe Broad Center of Regenerative Medicine and Stem Cell Research, University of California at Los Angeles, Los Angeles, California 90095, USA

[5]Department of Oral-Maxilla-facial Surgery, Shanghai Ninth Hospital, Shanghai Jiaotong University, Shanghai, China

[6]Department of Otolaryngology and Head and Neck Surgery, Affiliated Beijing Tongren Hospital, Capital University of Medical Sciences, Beijing, China

[7]Department of Pathology, David Geffen School of Medicine, University of California at Los Angeles, Los Angeles, California 90095, USA

Abstract

The transcription factor AP-1 (activator protein-1), a heterodimer of the JUN and FOS proteins, promotes the invasive growth and metastasis of various tumors such as squamous cell carcinoma (SCC), breast cancer and melanoma. AP-1 activity is transcriptionally induced through a positive-feedback loop. We identified the histone demethylase KDM4A (lysine-specific demethylase 4A) as a key epigenetic priming factor in this positive feedback loop. KDM4A contributed to the induction of genes encoding the AP-1 transcription factors and the invasive growth and metastasis of SCC. KDM4A knockdown decreased growth factor-induced mRNA expression and protein abundance of AP-1 family members, including JUN and FOSL1. Mechanistically, histone demethylation by KDM4A facilitated the binding of the AP-1 complex to the promoters of *JUN* and *FOSL1*, thereby promoting the positive feedback loop that maintains activation of AP-1. In a mouse model of SCC, KDM4A knockdown inhibited lymph node metastasis. Moreover, the abundance of KDM4A correlated with the abundance of JUN and FOSL1 in human SCC tissues and *KDM4A* expression was increased in human lymph node metastases. Our studies provide

[†]To whom correspondence should be addressed. Dr. Cun-Yu Wang, Division of Oral Biology and Medicine, Jonnson Comprehensive Cancer Center and School of Dentistry, UCLA, 10833 Le Conte Ave, Los Angeles, CA 90095-1668, Phone: 310-825-4415, cunywang@ucla.edu.
[*]These authors contributed equally to this work.

Author contributions: D.X, H.P., J.L. Q.Z. and X.C. performed experiments analyzed data, and prepared figures. S.D. prepared human SCC samples. C.Y.W. designed experiments, analyzed the data and wrote the manuscript.

Data and materials availability: Microarray data have been deposited in the Gene Expression Omnibus (GEO) under accession number GSE44238.

Competing interests: The authors declare that they have no competing financial interests.

insights into the epigenetic control of AP-1 and tumor invasion, and suggest that KDM4A could be an important therapeutic target for inhibiting invasive SCC growth and metastasis.

INTRODUCTION

The transcription factor AP-1 (activator protein 1) is one of the major effectors activated by signaling mediated by the hepatocyte growth factor (HGF) receptor tyrosine kinase (also known as MET or c-MET) and other oncogenic factors (1–4). It is well known that AP-1 plays a critical role in invasive tumor growth and metastasis. AP-1 consists of the different FOS and JUN (also known as c-Jun) dimers that bind to 12-O-tetradecanoylphorbol-13-acetate response elements, or AP-1 sites (5'-TGAG/CTCA-3'), to activate gene transcription. The FOS family of proteins includes FOS, FOSB, FOSL1 (also known as Fra-1) and FOSL2, and the JUN family of proteins contains JUN, JUNB, JUND and ATF (activating transcription factors) family members. AP-1 can be activated by phosphorylation of JUN and FOS or by multiple extracellular stimuli inducing the expression of JUN and FOS (4–6). JUN and FOSL1 positively regulate their own expression through AP-1 sites on their promoters (7, 8), thereby amplifying AP-1 activation. Among the AP-1 family members, JUN and FOSL1 have a critical role in the invasive growth and metastasis of human cancers such as squamous cell carcinoma (SCC), breast cancer and melanoma (4, 5).

SCC of the oral cavity, head, and neck is one of the most deadly and debilitating malignant tumors worldwide with a 5-year survival rate of only about 50% (10). This poor prognosis mainly results from the high invasive potential of these tumors, resulting in regional lymph node metastasis (9–11). Invasive growth is a complex process that involves cell proliferation, cell scattering and migration, and matrix degradation, enabling cells to penetrate the basement membrane and connective tissue and enter the lymphatic and vascular circulation. Invasive growth plays a critical role in the progression of carcinoma in situ to SCC and finally to lymph node metastasis (12, 13). Abnormal activation of the MET signaling pathway is associated with the invasion and metastasis of SCC (3, 13–19). HGF binds to MET and activates multiple intracellular signaling pathways, including those mediated by phosphatidylinositol 3 kinase (PI3K), mitogen-activated protein kinase (MAPK), and nuclear factor-kappa B (NF-κB), promoting human SCC cell scattering and invasion in vitro (14, 20). Increased abundance of MET is found in lymph node metastases compared with human primary SCC, and increased serum HGF is found in patients with regional lymph node metastasis from SCC (13, 15–17). Increased abundance of HGF or MET is correlated with poor prognosis in several human cancers, including head and neck SCC, breast, ovarian and non-small-cell lung cancers. Moreover, studies show that MET activity is increased in small-cell lung carcinomas treated with EGFR (epidermal growth factor receptor)-targeted therapies, creating drug resistance in patients (20). Therefore, understanding the MET signaling pathway may help to develop therapeutic strategies to prevent metastasis and overcome resistance.

The activation of AP-1 by HGF and other growth factors plays an important role in tumor invasion and metastasis (1–3, 5). Although substantial progress has been made in understanding the molecular control of SCC invasion and metastasis, very little is known about the epigenetic events that regulate these molecular mechanisms. Emerging evidence suggests that histone methylation plays a critical role in controlling gene transcription by altering chromatin accessibility (21, 22). A group of histone demethylases activate or inhibit gene transcription by removing histone methylation marks (21–23). To explore the epigenetic control of SCC invasion and metastasis, we performed a functional in vitro siRNA screen to identify histone demethylases that may be required for SCC invasion. We identified KDM4A (lysine-specific demethylase 4A, also known as JMJD2A) as a key

epigenetic factor that activated the expression of the *JUN* and *FOSL1* by removing trimethyl-lysine 9 of histone H3 (H3K9me3) from the genes' promoter regions, which enabled recruitment of AP-1 to the promoters of *JUN* and *FOSL1* and thereby promoted the activation of AP-1. Depletion of KDM4A significantly inhibited the metastasis of SCC to cervical lymph nodes in an orthotopic nude mouse model of SCC. Moreover, KDM4A abundance was significantly increased in human metastatic SCC in lymph nodes compared to primary human SCC and was positively correlated with the abundance of JUN and FOSL1, indicating that KDM4A has a critical role in activating AP-1 and promoting human SCC metastasis.

RESULTS

KDM4A Is Required for Oncogenic MET-induced SCC Invasion

Increased abundance of MET expression is frequently found in human head and neck SCC and other cancers such as lung, prostate, and breast cancers and is associated with tumor metastasis (9, 10, 12, 13, 18). Previously, we showed that the HGF-induced activation of MET promoted cell scattering and invasion of human SCC23 cells (1–3). To establish a robust cellular model system for screening genes associated with cell invasion, we overexpressed oncogenic translocated promoter region (TPR)-MET fusion proteins in SCC23 cells (SCC23/MET; Fig. 1A). TPR-MET constitutively activates the downstream intracellular signaling pathways of MET and facilitates cell transformation and invasion in vitro and in vivo (19). Whereas SCC23 cells expressing the empty vector (SCC23/V) formed compact epithelial islands, SCC23/MET cells dissociated from each other and exhibited a scattered phenotype similar to that induced by HGF (Fig. 1B). Both ERK (extracellular signal-regulated kinase) and the Akt kinase were constitutively activated in SCC23/MET cells, in which the phosphorylation of ERK and Akt was similar to that induced by HGF (Fig. 1C). Consistent with our previous studies, the abundance of JUN and FOSL1 (two key members of AP-1) was increased in SCC23/MET cells (Fig. 1C), indicating that AP-1 was activated by MET-mediated signaling. Furthermore, SCC23/MET cells were highly invasive compared with SCC23/V cells (Fig. 1, D and E), suggesting that SCC23/MET cells were a valid model for functional screening experiments.

To profile the role of histone demethylases in SCC invasion, SCC23/MET cells were transfected with a panel of siRNA, each targeting one of 27 histone demethylases, and knockdown was confirmed by real-time reverse transcription polymerase chain reaction (RT-PCR) (Fig. 1F). The expression of *UTY* and *KDM5D* in SCC23/MET cells was too low to be detected. Our initial screening found that the knockdown of *KDM4A*, *KDM4C*, *KDM2B*, *KDM6A*, *KDM8*, *JMJD6*, *JMJD7*, and *JMJD8* strongly inhibited SCC23/MET invasion by more than 80% (Fig. 1, G and H). We focused our work on *KDM4A*, because precise mechanisms for the demethylases encoded by *KDM4C*, *KDM2B*, *KDM6A*, *KDM8*, *JMJD6*, *JMJD7*, and *JMJD8* were not clear.

KDM4A Controls SCC Invasive Growth by Activating AP-1

KDM4A can activate or inhibit gene transcription by removing H3K9me3 and H3K36me3 marks (24–26). To confirm this in our studies, we generated two lentivirus-based shRNAs (sh1 and sh2) to target two different KDM4A sequences. Both KDM4Ash1 and KDM4Ash2 were able to knock down KDM4A in SCC23/MET cells (Fig. 2A). KDM4A knockdown drastically reduced SCC23/MET cell scattering (Fig. 2B) and invasion induced by the oncogenic MET (Fig. 2C). Whereas there was no difference in cell proliferation rates between SCC23/MET/V and SCC23/MET/KDM4Ash1 or SCC23/MET/KDM4Ash2 cells over 48 hours, SCC23/Met/KDM4Ash1 and SCC-23/MET/KDM4Ash2 cells grew more slowly than SCC23/MET/V cells over 72 hours in vitro (Fig. 2D). Because invasion assays

were performed in the first 24 hour period, it was unlikely that the inhibition of SCC23/MET invasion by KDM4A shRNA was an artifact of slower cell proliferation. Moreover, we found that the knockdown of KDM4A significantly inhibited SCC tumor growth in an orthotopic mouse model of head and neck SCC in which cells were submucosally inoculated into the floor of the mouth near the base of the tongue (Fig. 2E).

To explore how KDM4A epigenetically promoted SCC invasion, we performed gene profiling to screen for invasive genes that were affected by KDM4A knockdown. Microarray analysis revealed 159 genes which had decreased expression (table S1) and 59 genes which had increased expression (table S2) by at least two-fold after KDM4Ash2 knockdown. Gene enrichment analysis revealed that the knockdown of KDM4A significantly reduced the expression of the AP-1 family members, including *JUN*, *JUNB*, *FOSL1*, *FOSL2*, and *ATF-3*, and AP-1 target genes associated with lymph node metastasis, including *PLAUR* (urokinase plasminogen activation receptor), *VEGFA* (vascular endothelial growth factor A), *IL-8* (interleukin-8), and *CTGF* (connective tissue growth factor) (Fig. 3A), indicating that KDM4A is functionally required for AP-1 activation. Real-time RT-PCR confirmed that KDM4A knockdown inhibited the expression of AP-1 member genes as well as AP-1 target genes induced by MET (Fig. 3, B and C). A large number of studies show that JUN and FOSL1 are two key AP-1 members which play an important role in tumor invasion and metastasis (5, 6). Previously, we and others have shown that HGF-MET signaling activated AP-1 by inducing the transcription of *JUN* and *FOSL1* and stimulated human SCC invasive growth (1, 3, 27, 28). Moreover, increased abundance of FOSL1 is associated with lymph node metastasis of human SCC (28). AP-1 directly binds to the promoters of *JUN* and *FOSL1* and promotes the expression of *JUN* and *FOSL1*, thereby enhancing its own transcriptional activity (4). We hypothesized that KDM4A is a key epigenetic regulator which was required for the induction of JUN and FOSL1 in SCC cells. KDM4A knockdown by two different shRNA vectors reduced the abundance of JUN and FOSL1 in cells with activated MET (Fig. 2A). To exclude off-target effects, we also restored KDM4A in SCC23/MET/KDM4Ash2 cells using a shRNA-resistant construct. Western blot analysis showed that the restoration of KDM4A rescued the abundance of JUN and FOSL1 (Fig. 3D). Real-time RT-PCR also confirmed that the restoration of KDM4A reinstated *JUN* and *FOSL1* expression (Fig. 3, E and F). To determine whether the histone demethylase activity of KDM4A was required for the expression of *JUN* and *FOSL1*, we overexpressed a catalytically-dead KDM4A mutant (KDM4A-H188A) in SCC23/MET/KDM4Ash2 cells. In contrast to restoration with wild-type KDM4A, overexpression of KDM4A-H188A could not restore the expression of JUN and FOSL1 (Fig. 3, D to F), nor could it restore the invasive behavior of SCC23/MET/KDM4Ash2 cells (Fig. 3G), suggesting that the histone demethylase activity of KDM4A is essential for the expression of *JUN* and *FOSL1*.

To examine whether KDM4A was required for the HGF - induced mRNA and prot ein abundance of JUN and FOSL1, we knocked down KDM4A in parental SCC23 cells (Fig. 4A). The depletion of KDM4A in SCC23 cells significantly inhibited the abundance of JUN and FOSL1 induced by HGF at both the translational (Fig. 4A) and transcriptional levels (Fig. 4, B and C). To exclude off-target effects of shRNA, we also restored SCC23/KDM4Ash2 cells with KDM4A. The restoration of KDM4A reinstated the abundance of JUN and FOSL1 induced by HGF (fig. S1A). Consistently, overexpression of KDM4A in SCC23 cells also enhanced FOSL1 abundance induced by HGF (fig. S1B). To determine whether the findings for KDM4A applied to multiple SCC cell types, we knocked down KDM4A in two other head and neck SCC cell lines, FaDu and SCC1 (Fig. 4, D and E). Knockdown of KDM4A in FaDu and SCC1 cells suppressed the abundance of JUN and FOSL1 that was induced by HGF (Fig. 4, D and E). Matrigel invasion assays also confirmed that the knockdown of KDM4A in FaDu and SCC1 cells inhibited HGF-induced cell invasion (Fig. 4, F and G). Because KDM4A and KDM4C play similar functions in histone

modification, we also knocked down KDM4C in SCC23 and FaDu cells (fig. S2, A and B). In contrast to KDM4A knockdown, KDM4C depletion did not affect the abundance of JUN and FOSL1 induced by HGF (fig. S2, C and D), confirming that specifically KDM4A is crucial for the expression of *JUN* and *FOSL1*.

In addition to HGF, epidermal growth factor (EGF) also activates AP-1, and abnormal activation of EGF signaling is associated with progression and metastasis of head and neck SCC (5, 9, 10). Thus, we examined whether KDM4A was required for EGF-induced AP-1 activation. Whereas EGF potently induced the abundance of JUN and FOSL1 in SCC23/Scrsh and FaDu/Scrsh cells, the abundance of JUN and FOSL1 by EGF was suppressed by KDM4A depletion in both cell lines (Fig. 4, H and I). Together, our results suggest that KDM4A might play a broader role beyond HGF-MET signaling in the activation of AP-1 and SCC invasion.

Histone demethylation by KDM4A is required for AP-1 to bind to promoters

KDM4A primes gene transcription by removing repressive H3K9me3 marks in the chromatin (24–26). The promoters of *JUN* and *FOSL1* contain AP-1 sites, and JUN and FOSL1 regulate their own transcription through a positive feedback loop. To determine whether KDM4A epigenetically stimulated the expression of *JUN* and *FOSL1*, we first examined whether KDM4A was present on the promoters of *JUN* and *FOSL1* using chromatin immunoprecipitation (ChIP) assays. ChIP assays revealed that KDM4A was detected on the promoters of *JUN* and *FOSL1* in SCC23/MET/V cells, and that, as expected, KDM4A knockdown significantly reduced the binding of KDM4A to the promoter of *JUN* and *FOSL1* in SCC23/MET/KDM4Ash2 cells (Fig. 5, A and B). Consistently, decreased binding of KDM4A to the promoter regions was associated with increased occurrence of its substrate, H3K9me3, which is often a marker of gene silencing (Fig. 5, A and B). As a control, we could not detect KDM4A occupancy at 8 kb upstream of the transcription start sites in either SCC23/MET/V or SCC23/MET/KDM4Ash2 cells, and the knockdown of KDM4A did not affect the binding of H3K9me3 to that region (Fig. 5, A and B). KDM4A knockdown also modestly increased H3K36me3 on the promoters of *JUN* and *FOSL1* but not 8 kb upstream (Fig. 5, C and D). KDM4A knockdown did not cause global changes of the abundance of H3K9me3 and H3K36me3 (fig. S3A), nor did it affect the binding of H3K9me3 and H3K36me3 to the promoters of *AXIN2* and *DKK1* (fig. S3, B and C), which are specifically regulated by Wnt/β-catenin signaling but not by AP-1 (10, 11).

HGF did not appear to regulate the recruitment of KDM4A to the promoters of *JUN* and *FOSL1*, because KDM4A binding in either SCC23/Scrsh or SCC23/KDM4Ash2 cells was unaffected by the addition of HGF (Fig. 5, E and F). KDM4A knockdown increased the binding of H3K9me3 to the promoters of *JUN* and *FOSL1* regardless of HGF stimulation (Fig. 5, G and H), suggesting that the removal of H3K9me3 by KDM4A is required for HGF-induced AP-1 activation. KDM4A knockdown also modestly increased the binding of H3K36me3 to the promoters of *JUN* and *FOSL1* regardless of HGF stimulation (fig. S3, D and E). However, we could not predict the effect of demethylating H3K36me3 by KDM4A on the transcription of *JUN* and *FOSL1*.

Because the demethylase activity of KDM4A was required for the expression of *JUN* and *FOSL1*, we hypothesized that removal of H3K9me3 might be important for recruiting AP-1 to chromatin to activate transcription. Because co-immunoprecipitation assays did not detect the interaction between KDM4A and JUN, we performed re-ChIP assays to determine whether JUN and KDM4A co-occupied on the promoters of *JUN* and *FOSL1* in FaDu cells. Compared to the non-promoter region, HGF induced JUN to co-occupy the *FOSL1* promoter with KDM4A (Fig. 6, A and B). Similarly, HGF induced JUN to co-occupy the *JUN* promoter with KDM4A (Fig. 6, C and D). Because JUN and FOSL1 abundance were

induced in SCC23/MET cells, we also examined whether JUN and KDM4A co-occupied on the promoters of *JUN* and *FOSL1* in these cells. Compared to the non-promoter region, JUN- and KDM4A-associated chromatin complexes were present on the promoters of *FOSL1* (fig. S4, A and B) and *JUN* (fig. S4, C and D) in SCC23/MET cells.

Due to the fact that *JUN* expression was suppressed by KDM4A knockdown, we were unable to perform ChIP assays to determine whether histone demethylation by KDM4A was required for the recruitment of endogenous JUN to the promoters of *JUN* and *FOSL1*. To overcome this problem, we ectopically expressed JUN in both SCC23/Scrsh and SCC23/KDM4Ash2 cells in which JUN expression was constitutively driven by the CMV promoter independently of KDM4A (Fig. 6E). The recruitment of JUN to either the *JUN* or *FOSL1* promoter was significantly decreased in SCC23/KDM4Ash2/JUN cells compared with that in SCC23/Scrsh/JUN cells (Fig. 6, F and G). Consistently, whereas FOSL1 abundance was strongly induced by ectopic expression of JUN (in SCC23/Scrsh/JUN cells), FOSL1 induction was suppressed in these cells when KDM4A was depleted (SCC23/KDM4Ash2/JUN cells) (Fig. 6E). Real-time RT-PCR also confirmed that *FOSL1* mRNA induced by JUN was significantly decreased in SCC23/KDM4Ash2/JUN cells compared to SCC23/Scrsh/JUN cells (Fig. 6H). Moreover, HGF was also unable to induce FOSL1 abundance in SCC23/KDM4Ash2/JUN cells as strongly as it did in SCC23/Scrsh/V cells (fig. S5). The small induction of FOSL1 abundance might result from residual KDM4A after knockdown (Fig. 2A). Taken together, the results suggest that removal of H3K9me3 by KDM4A is required for the recruitment of AP-1 to the promoters of *JUN* and *FOSL1* to activate gene transcription.

KDM4A is required for human SCC lymph node metastasis in vivo

Head and neck SCC frequently through lymphatic rather than hematogenous dissemination (9, 10). Although several studies established a mouse model of SCC lymph node metastasis, most of the SCC cell lines used in those studies showed low frequency of metastasis to cervical lymph nodes (1, 29–31), potentially because these cell lines were not highly invasive or did not have abnormally activated MET. Because SCC23/MET cells were highly invasive and KDM4A knockdown suppressed invasion in vitro, we decided to examine whether KDM4A knockdown inhibited SCC23/MET cell metastasis in vivo. We modified an orthotopic mouse model of head and neck SCC in combination with in vivo and ex vivo bioluminescent imaging to detect cervical lymph node metastasis of SCC. Tumors derived from SCC23/MET/Scrsh cells were more metastatic than tumors from SCC23/MET/KDM4Ash2 cells when both tumors were grown for two weeks. Because this might be an artifact of the smaller tumors formed by SCC23/MET/KDM4Ash2 compared with SCC23/MET/Scrsh cells, SCC23/MET/KDM4Ash2-derived tumors were allowed to grow for longer periods of time until they were of similar size to SCC23/MET/Scrsh-derived tumors assessed by in vivo bioluminescent imaging: 20 days compared with 14 days, respectively (Fig. 7, A and B). Although in vivo bioluminescent imaging could in theory determine distant metastasis, it could not directly detect cervical lymph node metastasis, because mice were so small that primary tumors in the floor of the mouth masked cervical lymph node metastasis. Therefore, after sacrificing mice, cervical lymph nodes were immediately isolated and examined ex vivo using bioluminescent imaging. Cervical lymph nodes extracted from six out of eight mice with SCC23/MET/Scrsh-derived tumors, but only 2 out of 8 mice with SCC23/MET/KDM4Ash2-derived tumors, showed luciferase light emission indicating lymph node metastasis (Fig. 7, C and D). It is possible that we could not detect lymph node metastasis in the remaining two mice because they were culled at day 14 when tumor burdens in the oral cavity met their endpoint. Hematoxylin and eosin staining detected SCC lymph node metastasis in mice carrying Scrsh-derived tumors, and immunostaining for keratin, a marker for squamous cells, further confirmed SCC lymph node metastasis (Fig.

7E). The two incidences of lymph node metastasis from the KDM4A-depleted SCC cells were relatively small and may have been caused by inefficient KDM4A knockdown in some SCC cells, because metastatic tumor cells in the lymph nodes from these mice stained positively for KDM4A protein (fig. S6).

To further determine whether KDM4A epigenetically activated AP-1 to promote human SCC progression and metastasis, we compared KDM4A, JUN, and FOSL1 abundance in human SCC lymph node metastases with human primary SCC tissues and adjacent normal epithelial tissue. KDM4A, JUN, and FOSL1 abundance were significantly higher in human primary SCC tissues than in adjacent normal epithelial tissues (Fig. 7F and Table 1). Compared to human primary SCC tissues, the abundance of all three proteins were significantly increased in the majority of human SCC lymph node metastases, and KDM4A abundance positively correlated with the abundance of JUN (Table 2) and FOSL1 (Table 3), suggesting that KDM4A might promote SCC metastasis in human patients by activating AP-1. Supporting our findings is oncomine data analysis of two different reports (32, 33), which showed that the amount of *KDM4A* mRNA in human primary SCC tissues was significantly higher in patients with lymph node metastasis than in patients without lymph node metastasis (Fig. 7, G and H).

DISCUSSION

We identified KDM4A as an important epigenetic factor which promotes head and neck SCC invasion and metastasis by promoting the activation of AP-1. AP-1 activity can be regulated by posttranslational modifications, but the transcriptional and translational induction of AP-1 family members is critical for AP-1 activation (4–6). Although it is well-known how AP-1 transcriptionally regulates the expression of JUN and FOSL1 in a positive feedback loop (7, 8), our findings elucidate how the expression of JUN and FOSL1 are epigenetically regulated through KDM4A. Specifically, we showed that depletion of KDM4A can block the positive feedback loop driving AP-1 activation. KDM4A protein abundance was increased in human SCC compared with normal epithelia and was associated with human SCC metastasis, and its depletion reduced the invasive potential of SCC cells in vitro and in vivo. Our study provides new insights into the epigenetic and molecular control of AP-1 activation and human SCC metastasis.

The KDM4 family members include KDM4A, KDM4B, KDM4C and KDM4D. In addition to KDM4A, KDM4C knockdown also inhibited SCC invasion (Fig. 1G). KDM4C is highly expressed in oesophageal cancer, and the depletion of KDM4C inhibits esophageal carcinoma cell proliferation at the early time points (24). In contrast, KDM4A knockdown inhibited cell proliferation in long-term culture, suggesting that KDM4A may prevent or suppress signals related to contact inhibition. However, the depletion of KDM4C did not affect the abundance of JUN and FOSL1 induced by HGF-MET signaling (fig. S2, C and D), suggesting that KDM4A and KDM4C may target different sets of genes that promote SCC invasion. It is possible that KDM4C may directly promote the expression of invasive genes activated by AP-1. Further studies a r e needed to determine how KDM4C controls cell proliferation and invasion in human SCC and whether it promotes metastasis in vivo.

JUN and FOSL1 are the key members of AP-1 and are also directly induced by AP-1. Because JUN and FOSL1 are rapidly induced by growth factors, chromatin accessibility is critical for AP-1 binding to their promoters. ChIP assays demonstrated that demethylation of H3K9me3 by KDM4A was required for the recruitment of AP-1 to chromatin. AP-1 could not be recruited to the promoters of *JUN* and *FOSL1* in KDM4A-depleted SCC cells, and overexpression of the catalytically-dead KDM4A mutant could not restore MET-induced abundance of JUN and FOSL1, indicating that the histone demethylase activity of KDM4A

is essential for both AP-1 recruitment and its feedback activation loop. We also found that KDM4A knockdown modestly increased H3K36me3 on the promoters of *JUN* and *FOSL1*. H3K36me3 is associated with transcriptionally active genes (21–23). From this study, we could not predict the effect that the demethylation of H3K36me3 by KDM4A may have on the transcription of *JUN* and *FOSL1*. Regardless, our functional studies suggest that the removal of H3K9me3 by KDM4A played a dominant role in the activation of *JUN* and *FOSL1* transcription. Compared with normal epithelial tissues, KDM4A is more abundant in human metastatic SCC tissues. HGF did not induce the abundance of KDM4A (fig. S1A). Currently, it is unknown how KDM4A is increased in human SCC. We previously showed that *KDM4B* expression was induced by SMAD signaling in human mesenchymal stem cells (34). It will be interesting to examine whether SMAD signaling or other oncogenic factors regulate *KDM4A* expression.

Human SCC is highly invasive and frequently metastasizes to cervical lymph nodes. Human SCC metastasis may be promoted by a variety of growth factors or signaling pathways. Understanding the molecular and epigenetic mechanisms which control human SCC metastasis will help to develop new therapeutic strategies (9, 10). MET is also induced by hypoxia. Emerging evidence suggests that MET activation promotes resistance to cancer therapy (20). Our results demonstrate that KDM4A may be a critical target for inhibiting human SCC invasive growth and metastasis. Because KDM4A knockdown inhibited the activation of AP-1 induced not only by HGF-MET, but also by EGF (Fig. 4), targeting KDM4A might inhibit multiple signaling pathways that drive SCC growth, invasion, and metastasis. Although it is possible that decreased cell proliferation contributed to the suppression of SCC metastasis after KDM4A depletion, our findings suggest that KDM4A directly controls SCC invasion and metastasis through AP-1 because (i) KDM4A promoted SCC cell invasion and scattering that correlated with increased abundance of activity of AP-1 in vitro, and (ii) KDM4A abundance was increased in human SCC lymph node metastasis and correlated with the abundance of JUN and FOSL1 in human SCC tissues. Because histone demethylases are enzymes which can be readily inhibited by small molecule inhibitors, targeting KDM4A may help to prevent human SCC invasive growth and to inhibit SCC metastasis.

MATERIALS AND METHODS

Cell culture and viral transduction

Human head and neck SCC cell lines, SCC23, FaDu and SCC1 cells, were maintained in DMEM containing 10% FBS and antibiotics. The pBabe-TPR-MET was kindly provided by Dr. George Vande Woude, and pCMV-HA-KDM4A was purchased from Addgene and subcloned into the retroviral vector pQCXIH. For viral transduction, retrovirus was generated by co-transfection of pBabe-TPR-MET or pQCXIH-HA-KDM4A with packaging plasmids into HEK293T cells as described previously (35). To generate stable cell lines, we transduced SCC cells with the related virus particles and subsequently selected cells with antibiotics for at least ten days. To stably knockdown KDM4A, lentiviruses expressing KDM4Ash1 or KDM4Ash2 were packaged and generated in 293T cells as described previously (35–37). Cells were transfected with lentiviruses and selected with antibiotics for at least one week at which point knockdown was confirmed by real-time RT-PCR or Western blot analysis. The two shRNA targeting sequences for KDM4A were 5’-CGAGTTATCAACTCAAGAT-3’ (KDM4Ash1) and 5’-GCCACGAGCATCCTATGAT-3’ (KDM4Ash2).

siRNA screening, real-time RT-PCR and Matrigel invasion assays

All histone demethylase-targetd siRNA and scramble siRNA were purchased from Santa Cruz Biotechnology. Each siRNA consists of pools with three to five target-specific 19–25 nt siRNAs designed to knockdown target gene expression. SCC23/MET cells were transfected with siRNAs using Lipofectamine RNAiMax (Invitrogen). 36 hours after transfection, total RNA was isolated from cells using TRIzol reagent, and cDNA was synthesized with oligo(dT) primers using M-MuLV reverse transcriptase (NEB). Quantitative RT-PCR (qRT-PCR) analysis was carried out with iQ SYBR green supermix (Bio-Rad) on an iCycler iQ real-time PCR detection system (Bio-Rad). Primers for JUN were: forward, 5'-CTACAGTATTCAGGATCTTGGGGTTA-3'; reverse, 5'-ACCTTCTATGACGATGCCCTCA-3'. Primers for FOSL1 were: forward, 5'-AAGTGCAGGAACCGGAGGAAG; reverse, 5'-CGGAGTTCCAGTTTGTCAGTCTC CG-3'. Primers for ACTIN were: forward, 5'-CACTCTTCCAGCCTTCCTTC-3'; reverse, 5'- GGATGTCCACGTCACACTTC-3'. Primers for the human histone histone demethylases are in table S3. To screen cell invasion, 1×10^5 siRNA-transfected cells were plated on BD BioCoat Matrigel invasion chambers. After 24 hours, Matrigel was removed and the invaded cells were stained with the HEMA-3 kit (Fisher). The invaded cells were counted in 5 to 10 random fields and averaged. Each group was performed in triplicates.

Western blotting analysis

Cells were lysed in RIPA buffer [10 mM Tris-HCL, 1 mM EDTA, 1% sodium dodecyl sulfate (SDS), 1% Nonidet P-40, 1:100 protease inhibitor cocktail, 50 mM β-glycerophosphate, 50 mM sodium fluoride]. Whole cell lysates were run on a 10% SDS polyacrylamide gel and transferred to a PVDF membrane using a semi-dry transfer apparatus (Bio-Rad). Membranes were blotted with 5% milk for 2 hours and incubated with primary antibodies overnight. The immunocomplexes were detected with horseradish peroxidase (HRP)-conjugated anti-rabbit or anti-mouse IgG (Promega) and envisioned with SuperSignal reagents (Pierce) as previously described (35–37). Primary antibodies against the indicated proteins were purchased from the following sources and used at the indicated dilutions: FOSL1 (1:1000; Santa Cruz Biotechnology); JUN (1:1000; Cell Signaling Technology); KDM4A (1:1000; Cell Signaling Technology); α-tubulin (1:100,000 Sigma-Aldrich).

ChIP assays, human affymetrix microarray, and Oncomine data analysis

ChIP assays were carried out using a ChIP assay kit following the manufacturer's protocol (Upstate Biotechnology). Cells were treated with a dimethyl 3,3' dithiobispropionimidate-HCl (DTBP) solution (5 mmol; Pierce) for 10 min at room temperature, followed by formaldehyde treatment for 15 min in a 37°C water-bath. For each ChIP reaction, 2×10^6 cells were used. All resulting precipitated DNA samples were quantified with a specific set of primers for individual genes using real-time PCR: *FOSL1* AP-1 site, forward 5'-GGTCTTTCCACTGGCCTTGTTTTAAG-3' and reverse 5'-TGCCCATACATG GTGTAACTTCC-3'; *FOSL1* 8 kb upstream, forward 5'-GTTGAGAGTTCGAGACCAGC-3' and reverse 5'-ATTACAGTCACGCGCCACCACACCT-3'; *JUN* AP-1 site, forward 5'-TTCTAGGGTGGAGTCTCCATGGT-3' and reverse 5'-GCCCGAGCTCAACACTTATC-3'; *JUN* 8 kb upstream, forward 5-'GGACATGAGAATGTATCATTCCAGG-3' and reverse 5'-TGAGGTCAGAGCTAGGCTAATGGTT-3'. Data are expressed as the percentage of input DNA. Antibodies for ChIP assays were purchased from the following commercial sources: anti-H3K9me3 (Abcam), anti-H3K36me3 (Abcam), anti-KDM4A (Bethyl) anti-JUN (Abcam).

For microarray, total RNA was extracted with miRNeasy kit following the manufacturer's instruction (Qiagen). 5 μg aliquots of total RNAs were transcribed from each sample to double-stranded complementary DNA (cDNA) using SuperScript II RT (Invitrogen) with an oligo-dT primer and then used to generate single-stranded RNAs. The biotin-labeled RNAs were fragmented and hybridized with an Affymetrix Human Genome U133 Plus 2.0 Array at the UCLA DNA Microarray Facility. The arrays were scanned with the GeneArray scanner (Affymetrix). The robust multichip average (RMA) method was used to normalize the raw data.

For Oncomine data analysis, we analyzed KDM4A mRNA expression in head and neck cancers from two different studies (32, 33). Details of standardized normalization techniques and statistical calculations can be found on the Oncomine website. First, we applied standard analyses to raw microarray data using either the robust multichip average for Affymetrix data or the Loess normalization for cDNA arrays. To scale the data and allow comparison of multiple independent studies, we applied Z-score normalization by Oncomine. This included $\log^2$ transformation, setting the array median to 0, and standard deviation to 1. To determine whether KDM4A was differentially expressed, two-sided t tests were conducted using the SPSS 17.0 software (SPSS Inc.).

Orthotopic mouse model of head and neck SCC

All animal experiments were performed in accordance with a protocol approved by the UCLA committee on Animal Care. Both SCC23/MET/Scrsh and SCC23/MET/KDM4Ash cells (3×10^5 cells in 0.1 ml PBS) were submucosally inoculated into the floor of the mouth near the base of the tongue in 8–10 week-old nude mice (8 mice per group). Tumor growth was measured using bioluminescent imaging every three days after injection. Briefly, mice were anaesthetized with ketamine and xylazine, subsequently injected with D-luciferin (300 mg/kg in PBS), and imaged in an IVIS spectrum Xenogen machine (Caliper Life Sciences). Bioluminescent analysis was performed using the Living Image software according to the manufacturer's instruction (version 4.0, Caliper Life Sciences). To detect cervical lymph node metastasis, cervical lymph nodes from individual mice were harvested, incubated with D-luciferin solutions in a petri dish and then imaged in an IVIS spectrum Xenogen machine at the end of experiments. For the control group, mice (n = 8) were sacrificed for isolation of cervical lymph nodes at 14 days after inoculation. For the KDM4A knockdown group, mice (n = 8 mice) were sacrificed at 20 days after the inoculation in order to reach the similar tumor size as the control group.

Immunohistochemistry staining of human head and neck SCC

The utilization of human head and neck cancer samples for this study were approved by the UCLA Institutional Review Board. Paraffin-embedded sections provided by the UCLA Translational Pathological Core were deparaffinized with xylene twice and then rehydrated with distilled water through an ethanol series step by step. Tissue antigens were retrieved as described previously (2). The slides were stained with polyclonal antibodies against KDM4A (1:100; Bethyl), JUN (1:200; Cell Signaling Technology), and FOSL1 (1:100; Santa Cruz Biotechnology) or control IgG (Santa Cruz Biotechnology) at 4°C overnight. We then incubated sections with HRP-labeled polymer for 60 min, detected the immunocomplexes with AEC^+ chromogen (Dako EnVision System) and counterstained with hematoxylin QS. The intensity of immunostaining was scored as follows: 0, no staining; +, weak staining; ++, moderate staining; +++, strong staining. The Wilcoxon rank sum test was applied to test the significant differences in IHC staining intensity between different groups. The Pearson correlation coefficient of linear regression was used to determine the correlation between different proteins. All statistical analyses were performed using the SPSS 17.0 software.

Supplementary Material

Refer to Web version on PubMed Central for supplementary material.

Acknowledgments

We thank G. Vande Woude for reagents.

Funding: This work was supported by the National Institute of Dental and Craniofacial Research Grants (R37DE13848 and R01DE15964 to C.-Y.W.) and the Shapiro Family Charitable Foundation.

REFERENCES AND NOTES

1. Zeng Q, McCauley LK, Wang CY. Hepatocyte growth factor inhibits anoikis by induction of activator protein 1-dependent cyclooxygenase-2. Implication in head and neck squamous cell carcinoma progression. J Biol Chem. 2002; 277:50137–50142. [PubMed: 12393863]
2. Zeng Q, Li S, Chepeha DB, Giordano TJ, Li J, Zhang H, Polverini PJ, Nor J, Kitajewski J, Wang CY. Crosstalk between tumor and endothelial cells promotes tumor angiogenesis by MAPK activation of Notch signaling. Cancer Cell. 2005; 8:13–23. [PubMed: 16023595]
3. Zeng Q, Chen S, You Z, Yang F, Carey TE, Saims D, Wang CY. Hepatocyte growth factor inhibits anoikis in head and neck squamous cell carcinoma cells by activation of ERK and Akt signaling independent of NFkappa B. J Biol Chem. 2002; 277:25203–25208. [PubMed: 11994287]
4. Shaulian E, Karin M. AP-1 as a regulator of cell life and death. Nat Cell Biol. 2002; 4:E131–E136. [PubMed: 11988758]
5. Ozanne BW, McGarry L, Spence HJ, Johnston I, Winnie J, Meagher L, Stapleton G. Transcriptional regulation of cell invasion: AP-1 regulation of a multigenic invasion programme. Eur J Cancer. 2000; 36:1640–1648. [PubMed: 10959050]
6. Lopez-Bergami P, Lau E, Ronai Z. Emerging roles of ATF2 and the dynamic AP1 network in cancer. Nat Rev Cancer. 2010; 10:65–76. [PubMed: 20029425]
7. Adiseshaiah P, Peddakama S, Zhang Q, Kalvakolanu DV, Reddy SP. Mitogen regulated induction of FRA-1 proto-oncogene is controlled by the transcription factors binding to both serum and TPA response elements. Oncogene. 2005; 24:4193–4205. [PubMed: 15806162]
8. Angel P, Hattori K, Smeal T, Karin M. The jun proto-oncogene is positively autoregulated by its product, Jun/AP-1. Cell. 1988; 55:875–885. [PubMed: 3142689]
9. Haddad RI, Shin DM. Recent advances in head and neck cancer. N Engl J Med. 2008; 359:1143–1154. [PubMed: 18784104]
10. Leemans CR, Braakhuis BJ, Brakenhoff RH. The molecular biology of head and neck cancer. Nat Rev Cancer. 2011; 11:9–22. [PubMed: 21160525]
11. Comoglio PM, Trusolino L. Invasive growth: from development to metastasis. J Clin Invest. 2002; 109:857–862. [PubMed: 11927611]
12. Jeffers M, Fiscella M, Webb CP, Anver M, Koochekpour S, Vande Woude GF. The mutationally activated Met receptor mediates motility and metastasis. Proc Natl Acad Sci U S A. 1998; 95:14417–14422. [PubMed: 9826715]
13. Cortesina G, Martone T, Galeazzi E, Olivero M, De Stefani A, Bussi M, Valente G, Comoglio PM, Di Renzo MF. Staging of head and neck squamous cell carcinoma using the MET oncogene product as marker of tumor cells in lymph node metastases. Int J Cancer. 2000; 89:286–292. [PubMed: 10861506]
14. Di Renzo MF, Olivero M, Martone T, Maffe A, Maggiora P, Stefani AD, Valente G, Giordano S, Cortesina G, Comoglio PM. Somatic mutations of the MET oncogene are selected during metastatic spread of human HNSC carcinomas. Oncogene. 2000; 19:1547–1555. [PubMed: 10734314]
15. Marshall DD, Kornberg LJ. Overexpression of scatter factor and its receptor (c-met) in oral squamous cell carcinoma. Laryngoscope. 1998; 108:1413–1417. [PubMed: 9738769]
16. Qian CN, Guo X, Cao B, Kort EJ, Lee CC, Chen J, Wang LM, Mai WY, Min HQ, Hong MH, Vande Woude GF, Resau JH, Teh BT. Met protein expression level correlates with survival in

patients with late-stage nasopharyngeal carcinoma. Cancer Res. 2002; 62:589–596. [PubMed: 11809714]

17. Seiwert TY, Jagadeeswaran R, Faoro L, Janamanchi V, Nallasura V, El Dinali M, Yala S, Kanteti R, Cohen EE, Lingen MW, Martin L, Krishnaswamy S, Klein-Szanto A, Christensen JG, Vokes EE, Salgia R. The MET receptor tyrosine kinase is a potential novel therapeutic target for head and neck squamous cell carcinoma. Cancer Res. 2009; 69:3021–3031. [PubMed: 19318576]
18. Park M, Dean M, Kaul K, Braun MJ, Gonda MA, Vande Woude G. Sequence of MET protooncogene cDNA has features characteristic of the tyrosine kinase family of growth-factor receptors. Proc Natl Acad Sci U S A. 1987; 84:6379–6383. [PubMed: 2819873]
19. Dean M, Park M, Vande Woude GF. Characterization of the rearranged tpr-met oncogene breakpoint. Mol Cell Biol. 1987; 7:921–924. [PubMed: 3821733]
20. Blumenschein GR Jr, Mills GB, Gonzalez-Angulo AM. Targeting the hepatocyte growth factor-cMET axis in cancer therapy. J Clin Oncol. 2012; 30:3287–3296. [PubMed: 22869872]
21. Shi Y, Whetstine JR. Dynamic regulation of histone lysine methylation by demethylases. Mol Cell. 2007; 25:1–14. [PubMed: 17218267]
22. Klose RJ, Zhang Y. Regulation of histone methylation by demethylimination and demethylation. Nat Rev Mol Cell Biol. 2007; 8:307–318. [PubMed: 17342184]
23. Kooistra SM, Helin K. Molecular mechanisms and potential functions of histone demethylases. Nat Rev Mol Cell Biol. 2012; 13:297–311. [PubMed: 22473470]
24. Cloos PA, Christensen J, Agger K, Maiolica A, Rappsilber J, Antal T, Hansen KH, Helin K. The putative oncogene GASC1 demethylates tri- and dimethylated lysine 9 on histone H3. Nature. 2006; 442:307–311. [PubMed: 16732293]
25. Whetstine JR, Nottke A, Lan F, Huarte M, Smolikov S, Chen Z, Spooner E, Li E, Zhang G, Colaiacovo M, Shi Y. Reversal of histone lysine trimethylation by the JMJD2 family of histone demethylases. Cell. 2006; 125:467–481. [PubMed: 16603238]
26. Klose RJ, Yamane K, Bae Y, Zhang D, Erdjument-Bromage H, Tempst P, Wong J, Zhang Y. The transcriptional repressor JHDM3A demethylates trimethyl histone H3 lysine 9 and lysine 36. Nature. 2006; 442:312–316. [PubMed: 16732292]
27. Dong G, Chen Z, Li ZY, Yeh NT, Bancroft CC, Van Waes C. Hepatocyte growth factor/scatter factor-induced activation of MEK and PI3K signal pathways contributes to expression of proangiogenic cytokines interleukin-8 and vascular endothelial growth factor in head and neck squamous cell carcinoma. Cancer Res. 2001; 61:5911–5918. [PubMed: 11479233]
28. Zhang L, Pan HY, Zhong LP, Wei KJ, Yang X, Li J, Shen GF, Zhang Z. Fos-related activator-1 is overexpressed in oral squamous cell carcinoma and associated with tumor lymph node metastasis. J Oral Pathol Med. 2010; 39:470–476. [PubMed: 20149058]
29. Myers JN, Holsinger FC, Jasser SA, Bekele BN, Fidler IJ. An orthotopic nude mouse model of oral tongue squamous cell carcinoma. Clin Cancer Res. 2002; 8:293–298. [PubMed: 11801572]
30. Mangone FR, Brentani MM, Nonogaki S, Begnami MD, Campos AH, Walder F, Carvalho MB, Soares FA, Torloni H, Kowalski LP, Federico MH. Overexpression of Fos-related antigen-1 in head and neck squamous cell carcinoma. Int J Exp Pathol. 2005; 86:205–212. [PubMed: 16045542]
31. Ondrey FG, Dong G, Sunwoo J, Chen Z, Wolf JS, Crowl-Bancroft CV, Mukaida N, Van Waes C. Constitutive activation of transcription factors NF-(kappa)B, AP-1, and NF-IL6 in human head and neck squamous cell carcinoma cell lines that express pro-inflammatory and pro-angiogenic cytokines. Mol Carcinog. 1999; 26:119–129. [PubMed: 10506755]
32. Toruner GA, Ulger C, Alkan M, Galante AT, Rinaggio J, Wilk R, Tian B, Soteropoulos P, Hameed MR, Schwalb MN, Dermody JJ. Association between gene expression profile and tumor invasion in oral squamous cell carcinoma. Cancer Genet Cytogenet. 2004; 154:27–35. [PubMed: 15381369]
33. Ye H, Yu T, Temam S, Ziober BL, Wang J, Schwartz JL, Mao L, Wong DT, Zhou X. Transcriptomic dissection of tongue squamous cell carcinoma. BMC Genomics. 2008; 9:69. [PubMed: 18254958]
34. Ye L, Fan Z, Yu B, Chang J, Al Hezaimi K, Zhou X, Park NH, Wang CY. Histone demethylases KDM4B and KDM6B promotes osteogenic differentiation of human MSCs. Cell Stem Cell. 2012; 11:50–61. [PubMed: 22770241]

35. Park BK, Zhang H, Zeng Q, Dai J, Keller ET, Giordano T, Gu K, Shah V, Pei L, Zarbo RJ, McCauley L, Shi S, Chen S, Wang CY. NF-kappaB in breast cancer cells promotes osteolytic bone metastasis by inducing osteoclastogenesis via GM-CSF. Nat Med. 2007; 13:62–69. [PubMed: 17159986]

36. Rehman AO, Wang CY. CXCL12/SDF-1 alpha activates NF-kappaB and promotes oral cancer invasion through the Carma3/Bcl10/Malt1 complex. Int J Oral Sci. 2009; 1:105–118. [PubMed: 20695076]

37. Li J, Wang CY. TBL1-TBLR1 and beta-catenin recruit each other to Wnt target-gene promoter for transcription activation and oncogenesis. Nat Cell Biol. 2008; 10:160–169. [PubMed: 18193033]

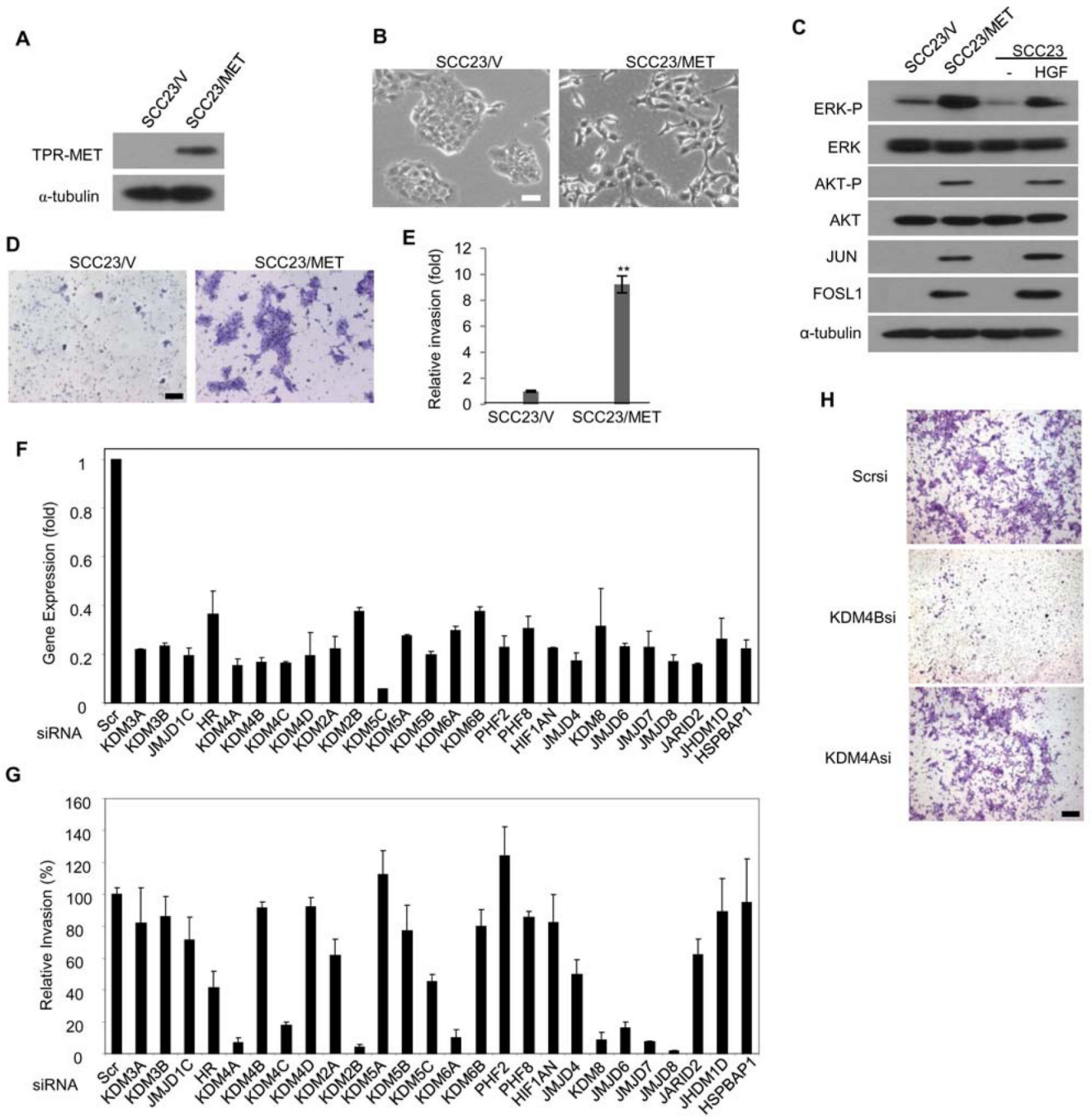

Fig 1. Histone demethylases are required for MET-induced SCC invasion in vitro

(**A**) Western blot analysis of the abundance of MET in SCC23 cells stably expressing TPR-tagged MET (SCC23/MET) or an empty vector (SCC23/V). (**B**) Light microscopy of SCC23/V and SCC23/MET cells representative of 3 independent transductions. Scale bar, 20 μm. (**C**) Western blot analysis of the phosphorylation and abundance of the indicated proteins in SCC23/V, SCC23/MET, and parental SCC23 cells [either untreated (−) or treated with 20 ng/ml of HGF for 30 min]. (**D**) Images and and (**E**) analysis of invasion assays with SCC23/V and SCC23/MET cells. Invasive cells were counted in 4 fields (n = at least 3 independent experiments). Data are means ± s.d. for triplicate samples from a representative

experiment. **$P<0.01$, unpaired two-tailed Student's *t*-test. Scale bar, 50 μm. (**F**) Real-time RT-PCR analysis of the relative expression of histone demethylases in human SCC23/MET cells treated with targeted siRNA relative to their expression in cells treated with scrambled (Scr) siRNA. Data are means ± s.d. of 3 experiments. (**G**) Analysis of invasion in SCC23/MET cells treated with the indicated siRNA relative to those treated with Scr siRNA. Invasive cells from 5 to 10 fields were quantified (n = 3 independent experiments). Data are means ± s.d. from a representative experiment. (**H**) Representative images (n = 3) from (G) in cells treated with scrambled siRNA (Scrsi) or siRNA targeting either KDM4A (KDM4Asi) or KDM4B (KDM4Bsi).

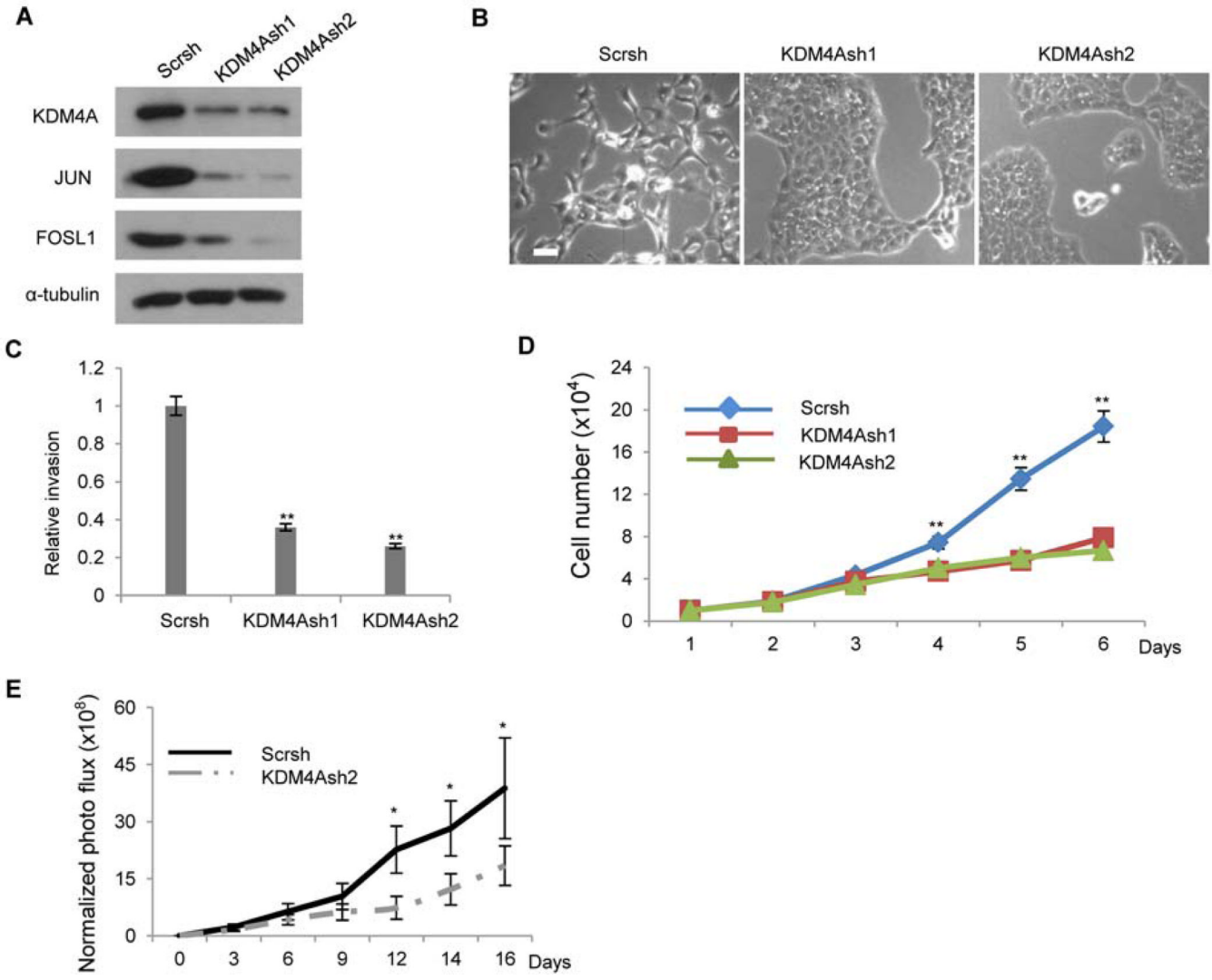

Fig 2. The knockdown of KDM4A inhibits SCC invasion in vitro and tumor growth in vivo

(**A**) Western blot analysis of the abundance of KDM4A, JUN and FOSL1 in SCC23/MET cells stably expressing one of two shRNA vectors targeting KDM4A (KDM4Ash1, KDM4Ash2) or a non-targeted (Scr) vector. (**B**) Representative images (n = 3) of cell scattering of cells described in (A). (**C**) Analysis of invasion using cells described in (A). Data are mean ± s.d. for triplicate samples from a representative experiment (n = 3). ***P*<0.01, unpaired two-tailed Student's *t*-test. (**D**) Cell proliferation analysis of cells described in (A). ***P*<0.01, unpaired two-tailed Student's *t*-test (n = 3). (**E**) The growth of xenograft tumors derived from either SCC23/MET/Scrsh or SCC23/MET/KDM4Ash2 cells assessed by bioluminescent imaging in mice. Data are means ± s.d. of the growth of tumors (6 mice per group) from a representative of 2 independent experiments. ***P*<0.05, unpaired two-tailed Student's *t*-test.

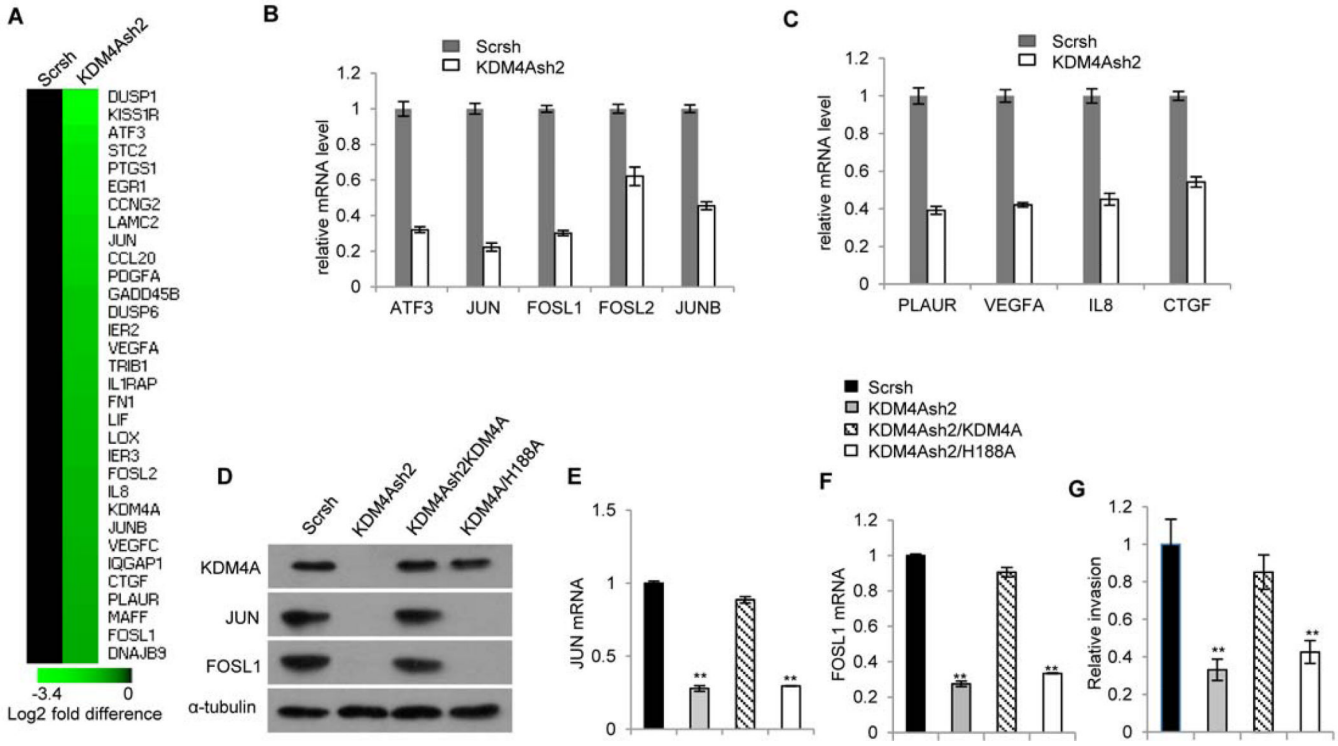

Fig 3. KDM4A controls AP-1 activation in SCC cells

(**A**) Gene expression profiling of AP-1 target genes in SCC23/MET cells transduced with nonspecific (Scrsh) or KDM4A-specfic (KDM4Ash2) shRNA. Black indicates no change in expression, whereas green indicates decreased expression, with magnitude indicated by lighter shades of green. (**B** and **C**) Real-time RT-PCR analysis of the expression of (**B**) AP-1 family genes *JUN*, *JUNB*, *FOSL1*, *FOSL2*, and *ATF3* and (**C**) AP-1 target genes *PLAUR*, *VEGFA*, *IL-8*, and *CTGF* in cells described in (A). (**D**) Western blot analysis of the abundance of JUN and FOSL in KDM4A-depleted (KDM4Ash 2) SCC/MET cells compared with their abundance in KDM4A-depleted SCC/MET cells transduced with either wild-type (KDM4Ash 2/KDM4A) or enzyme-inactive mutant (KDM4Ash 2/H188A) HA-tagged KDM4A. (**E** to **G**) Real-time RT-PCR analysis of *JUN* (**E**) or *FOSL* (**F**) expression, and invasive activity (**G**), in cells described in (D). ***P*<0.01, unpaired two-tailed Student *t*-test (n = 3).

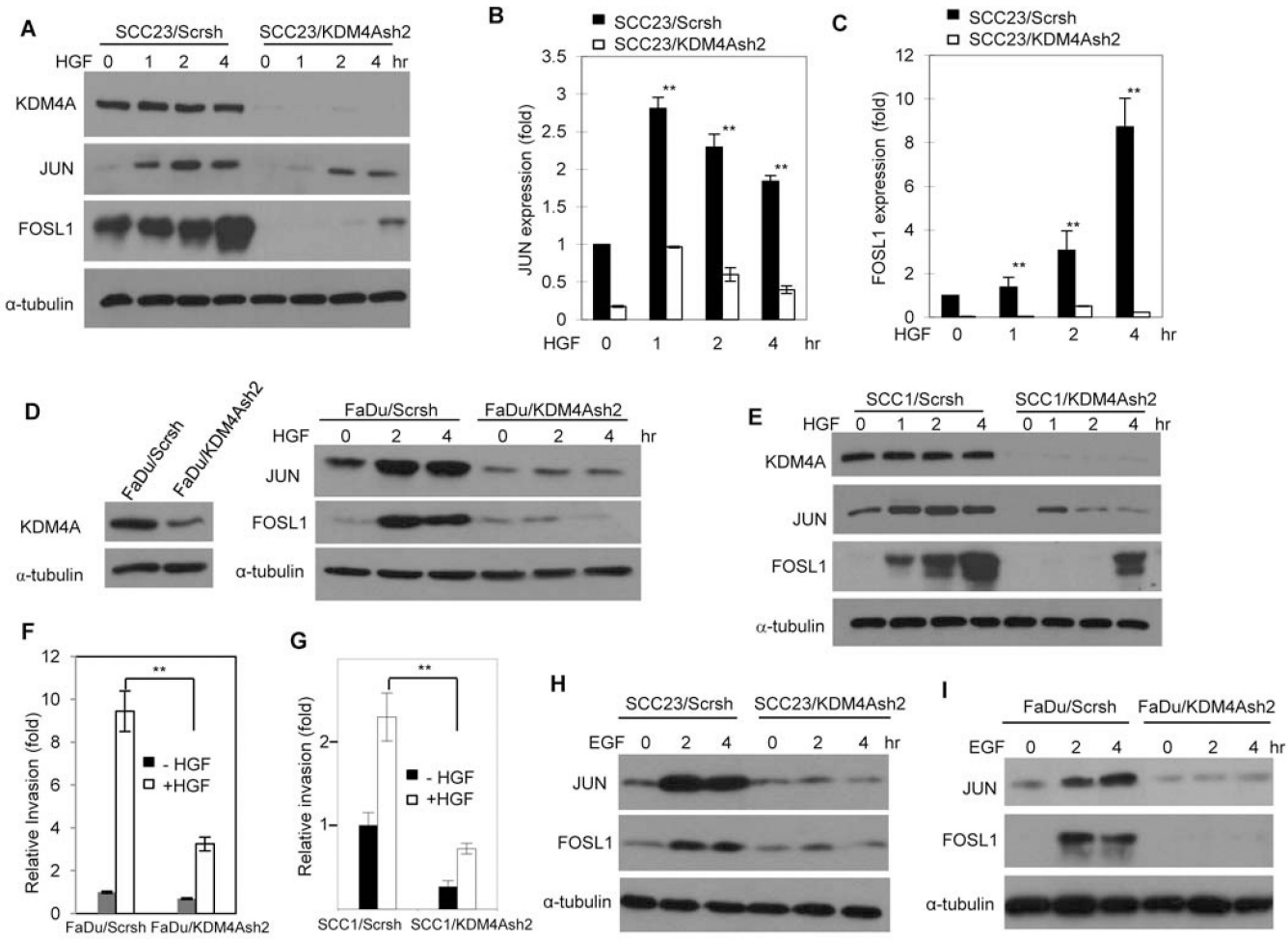

Fig 4. KDM4A is required for HGF-induced AP-1 and SCC cell invasion

(**A**) Western blot analysis of the abundance of JUN and FOSL1 in KDM4A-depleted (KDM4Ash2) and control (Scrsh) SCC23 cells treated with 20 ng/ml HGF for up to 4 hours. Data is representative of 2 independent experiments. (**B** and **C**) Real-time RT-PCR analysis of (**B**) *JUN* and (**C**) *FOSL1* expression in the cells described in (A). ***P*<0.01, unpaired two-tailed Student's *t*-test (n = 3). (**D and E**) Western blot analysis of the abundance of JUN and FOSL1 in KDM4A-depleted (KDM4Ash2) and control (Scrsh) FaDu (**D**) or SCC1 (**E**) cells treated with HGF. Blots are representative of 2 experiments. (**F** and **G**) Matrigel invasion assays of KDM4A-depleted or control FaDu (**F**) or SCC1 (**G**) cells treated with HGF. ***P*<0.01, unpaired two-tailed Student's *t*-test (n = 3). (**H** and **I**) Western blot analysis of JUN and FOSL1 abundance in KDM4A-depleted and control SCC23 (**H**) and FaDu (**I**) cells treated with 10 ng/ml EGF. Blots are representative of 2 experiments.

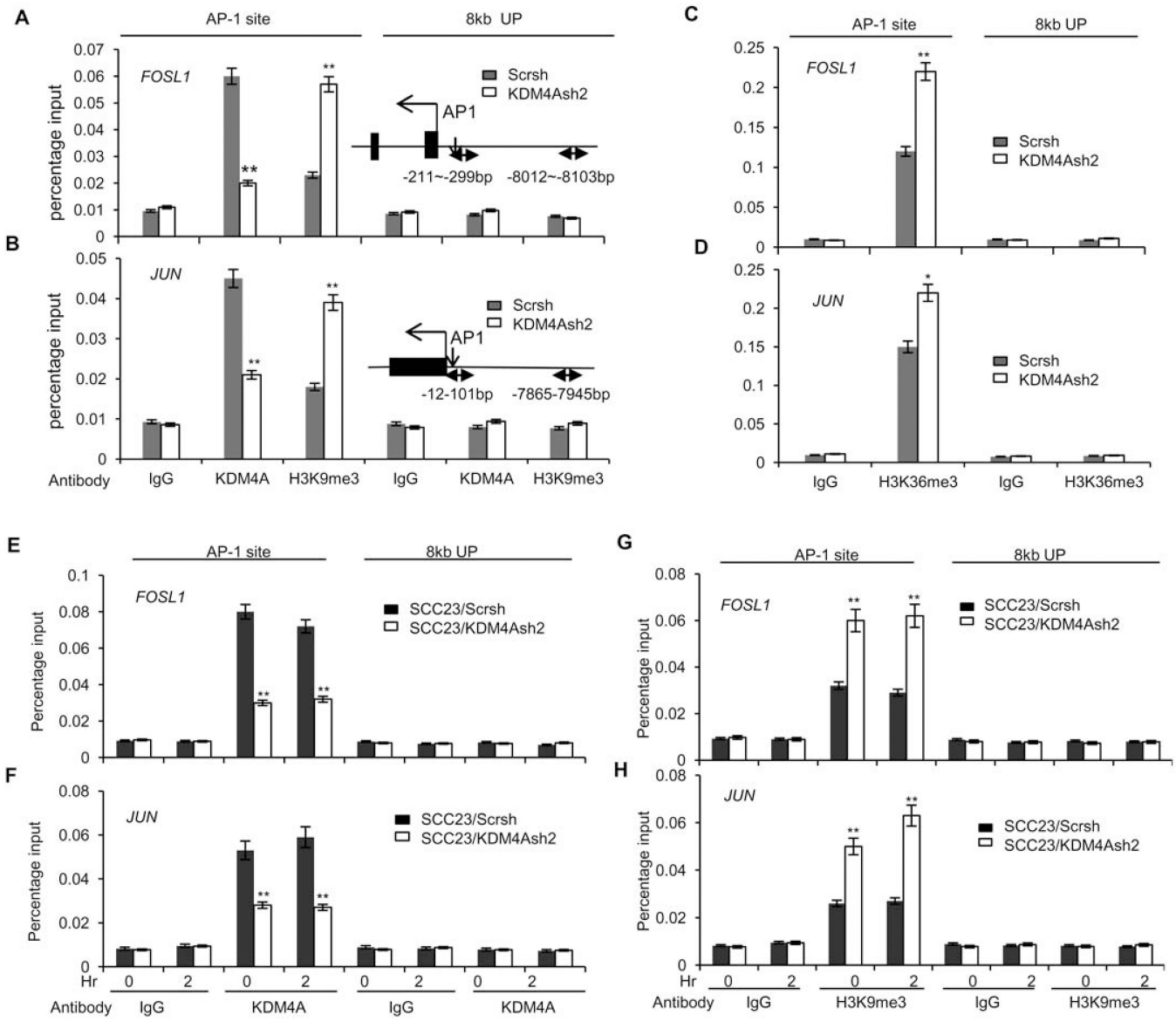

Fig 5. KDM4A binds to the promoters of *JUN* and *FOSL1* and demethylates H3K9me3 and H3K36me3 marks

(**A** and **B**) ChIP assays of KDM4A and H3K9me3 abundance on the (**A**) *FOSL1* or (**B**) *JUN* promoter, either on the AP-1 binding site or 8 kb upstream in SCC23/MET cells depleted of KDM4A (KDM4Ash2) compared with controls (Scrsh). ***P*<0.01, unpaired two-tailed Student's *t* test (n = 3). (**C** and **D**) ChIP assays of H3K36me3 abundance on the (**C**) *FOSL1* or (**D**) *JUN* promoter as described in (A) and (B). ***P*<0.01, **P*<0.05, unpaired two-tailed Student's *t*-test (n = 3). (**E** and **F**) ChIP assays of KDM4A abundance on the (**E**) *FOSL1* or (**F**) *JUN* promoter either on the AP-1 binding site or 8 kb upstream in SCC23 cells depleted of KDM4A (KDM4Ash2) and treated with 20 ng/ml HGF for up to 2 hours compared with treated control cells (Scrsh). ***P*<0.01, unpaired two-tailed Student's *t*-test (n = 3). (**G** and **H**) ChIP assays of H3K9me3 changes on the (**G**) *FOSL1* and (**H**) *JUN* promoter as described in (E) and (F). ***P*<0.01, unpaired two-tailed Student's *t*-test (n = 3).

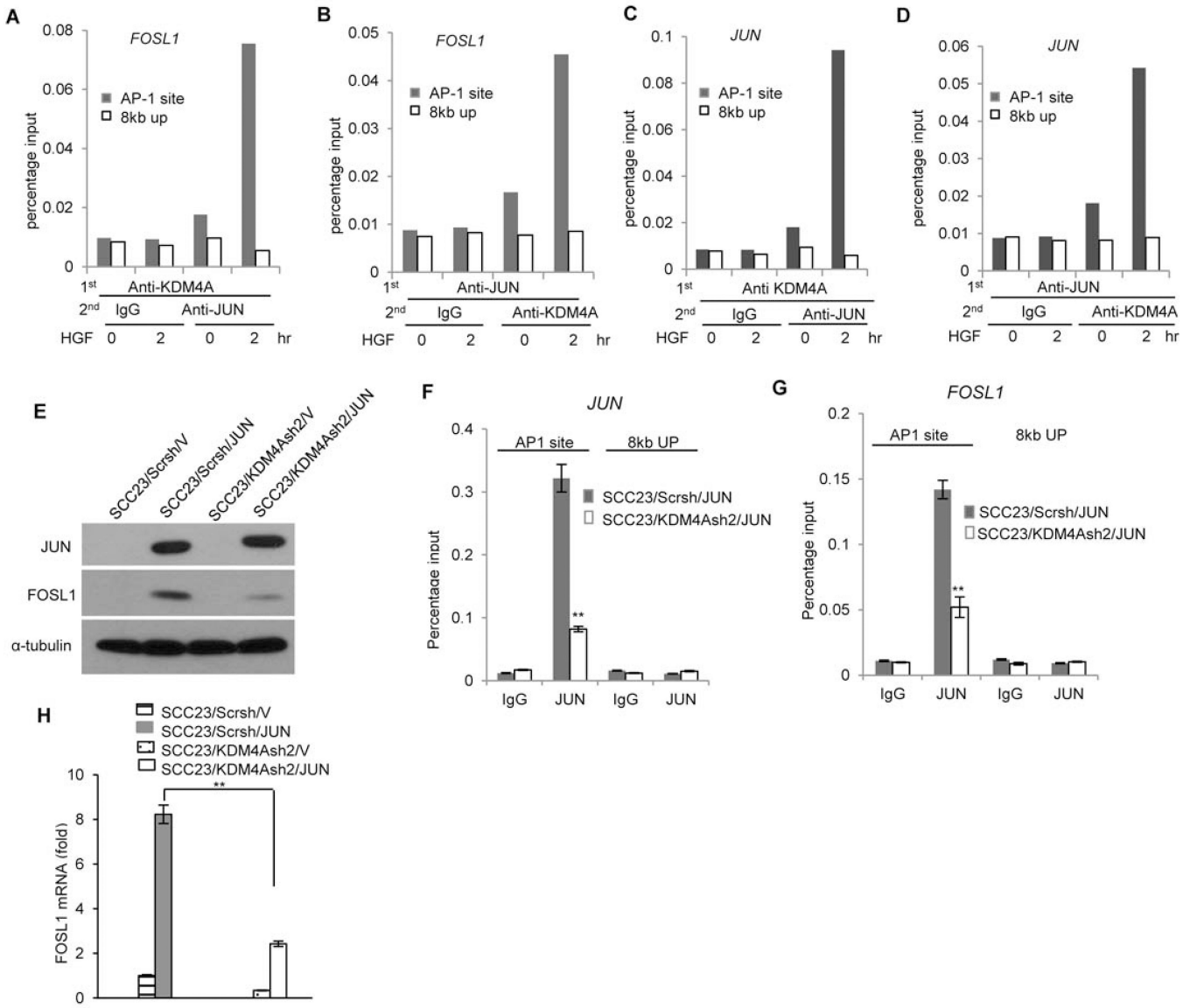

Fig 6. Histone demethylation by KDM4A is required for the recruitment of JUN/AP-1 to the target gene promoter

(**A** and **B**) Reciprocal re-ChIP assays of the co-occupancy of JUN and KDM4A on the *FOSL1* promoter in FaDu cells treated with 20 ng/ml HGF for up to 2 hours. Data represent three independent experiments. (**C** and **D**) Reciprocal re-ChIP assays of the co-occupancy of JUN and KDM4A on the *JUN* promoter as described in (A) and (B). Data represent three independent experiments. (**E**) Western blot analysis of JUN and FOSL1 abundance in SCC23 cells overexpressing JUN (Scrsh/JUN), depleted of KDM4A (KDM4Ash2/V), or overexpressing JUN in a KDM4A-depleted background (KDM4Ash2/JUN) compared with control cells (Scrsh/V). Blot is representative of 2 experiments. (**F** and **G**) ChIP assays of JUN abundance on the (**F**) *JUN* or (**G**) *FOSL1* promoter either at the AP-1 binding site or 8 kb upstream in SCC23 cells overexpressing JUN (Scrsh/JUN) compared with those also depleted of KDM4A (KDM4Ash2/JUN). ***P*<0.01, unpaired two-tailed Student's *t*-test (n = 3). (**H**) Real-time RT-PCR analysis of *FOSL1* expression in cells as described in (E). ***P*<0.01, unpaired two-tailed Student's *t*-test (n = 3).

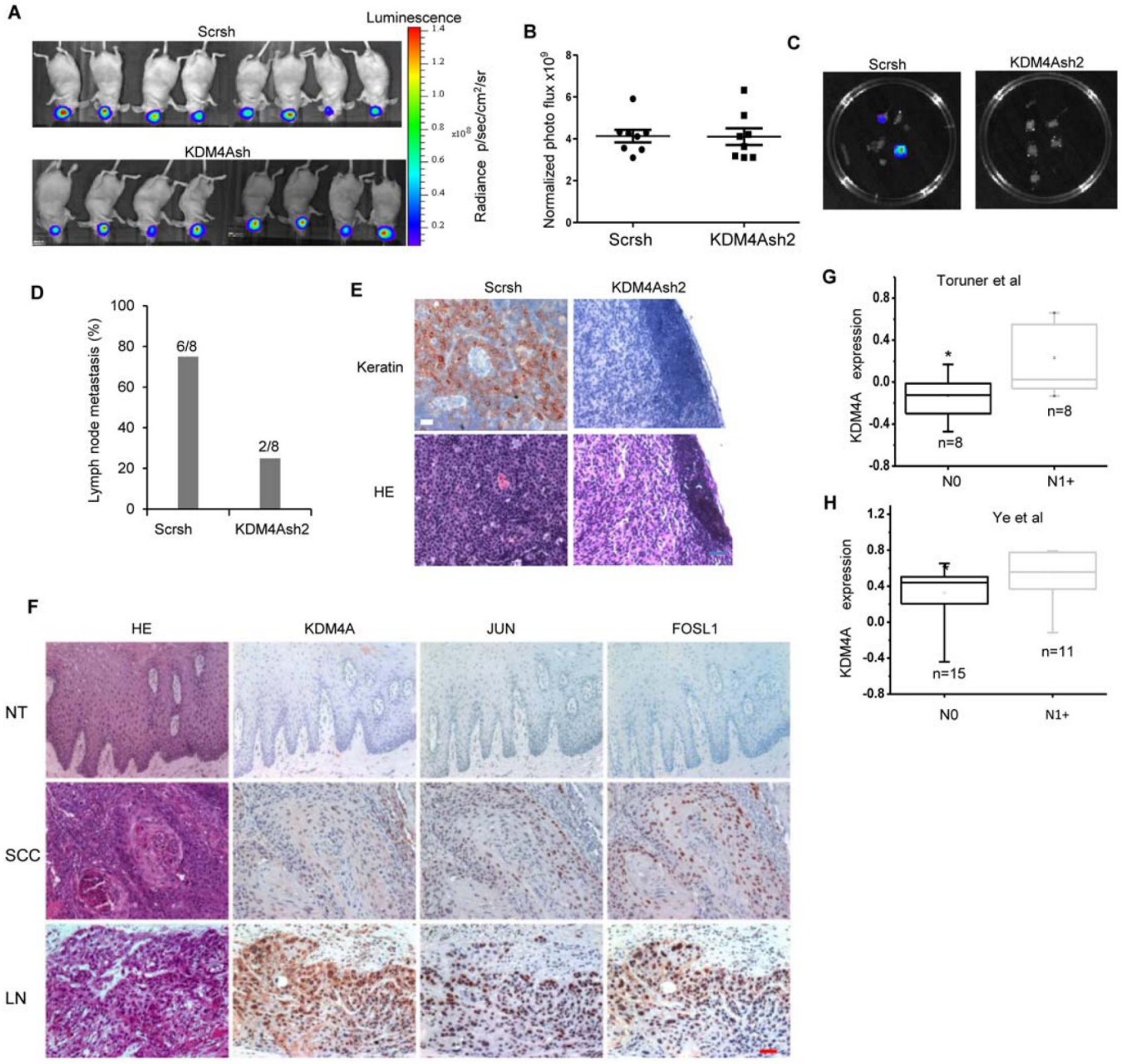

Fig 7. KDM4A is required for human SCC lymph node metastasis in vivo

(**A** and **B**) Xenograft tumors derived from SCC/MET/Scrsh cells (n = 8) or SCC23/MET/KDM4Ash2 cells (n = 8) in the oral cavity of mice was assessed by bioluminescent imaging for 14 or 20 days, respectively. Data are representative of two independent experiments. (**C**) Lymph node metastasis resulting from tumors in (A) assessed ex vivo by bioluminescent imaging. (**D**) Number and percentage of mice with lymph node metastasis from xenograft tumors described in (A). ***P*< 0.01, Fisher's exact test. (**E**) Histochemical detection of SCC lymph node metastases from (D) using an antibody against Pan-keratin. H&E staining provided for histology. Images are representative of −6 metastatic samples derived from SCC23/MET/Scrsh cells and 6 non-metastatic samples from SCC23/MET/KDM4Ash2 cells. Scale bar = 50 μm. (**F**) Histochemical detect ion of KDM4A, JUN, and FOSL1 abundance in

human SCC tissue (SCC) and SCC lymph node metastases (LN) compared with adjacent normal epithelial tissue (NT). Images are representative of 35 (NT), 68 (SCC), and 34 (LN) samples. (**G** and **H**) Oncomine analysis of *KDM4A* mRNA abudance in human primary SCC with lymph node metastasis (N1+) compared with human primary SCC without metastasis (N0) reported in (**G**) Toruner *et al*. (32) and (**H**) Ye *et al*. (33). **P*<0.05, unpaired two-tailed Student's *t*-tests.

Table 1

KDM4A is highly abundant in human SCC lymph node metastasis

	KDM4A				JUN				FOSL1			
	0	+	++	+++	**0**	+	++	+++	**0**	+	++	+++
Normal	45.71% (16/35)	42.86% (15/35)	11.43% (4/35)	0% (0/35)	62.86% (22/35)	37.14% (13/35)	0% (0/35)	0% (0/35)	45.71% (16/35)	42.86% (15/35)	11.43% (4/35)	0% (0/35)
SCC**	7.35% (5/68)	26.47% (18/68)	39.71% (27/68)	26.47% (18/68)	16.18% (11/68)	20.58% (14/68)	41.18% (28/68)	22.06% (15/68)	17.65% (12/68)	35.29% (24/68)	27.94% (19/68)	19.12% (13/68)
LN*	0% (0/34)	11.76% (4/34)	32.36% (11/34)	55.88% (19/34)	2.94% (1/34)	17.65% (6/34)	26.47% (9/34)	52.94% (18/34)	2.94% (1/34)	11.76% (4/34)	47.06% (16/34)	38.24% (13/34)

Normal human adjacent epithelial tissues (Normal; n = 35), human primary SCC without lymph node metastasis (SCC; n = 68), and metastatic SCC in lymph node (LN; n = 34) were stained for KDM4A, JUN, and FOSL1. The staining intensity was scored as: 0, negative staining; +, weak staining; ++, moderate staining; +++ strong staining.

** $P<0.01$ SCC versus normal;

* $P<0.05$ LN versus SCC; Wilcoxon rank sum test.

Table 2

The abundance of KDM4A correlates with the abundance of JUN in human SCC

		KDM4A**				Total
		0	+	++	+++	
JUN	0	21	13	0	0	34
	+	0	24	9	0	33
	++	0	0	19	18	37
	+++	0	0	14	19	33
Total		21	37	42	37	137

Normal adjacent tissues (n = 35), SCC (n = 68), and metastatic SCC in lymph node (n = 34) were stained for KDM4A and JUN. The staining intensity was scored as detailed in Table 1. Pearson correlation $R^2 = 0.872$,

** $P < 0.001$.

Table 3

The abundance of KDM4A correlates with the abundance of FOSL1 in human SCC

		KDM4A**				
		0	**+**	**++**	**+++**	**Total**
FOSL1	0	21	8	0	0	29
	+	0	29	10	4	43
	++	0	0	24	15	39
	+++	0	0	8	18	26
Total		21	37	42	37	137

Normal adjacent tissues (n = 35), SCC (n = 68), and metastatic SCC in lymph node (n = 34) were stained for KDM4A and FOSL1. The staining intensity was scored as detailed in Table 1. Pearson correlation R2 = 0.854,

** $P < 0.001$.